Unconventional Route to Encapsulated Ultrasmall Gold Nanoparticles for High-Temperature Catalysis

Tingting Zhang,[†] Hongyu Zhao,[†] Shengnan He,[†] Kai Liu,[†] Hongyang Liu,[‡,*] Yadong Yin,[§,*] and Chuanbo Gao[†,*]

[†]Center for Materials Chemistry, Frontier Institute of Science and Technology, Xi'an Jiaotong University, Xi'an, Shaanxi 710054, China, [‡]Shenyang National Laboratory for Materials Science, Institute of Metal Research, Chinese Academy of Sciences, Shenyang, Liaoning 110016, China, and [§]Department of Chemistry, University of California, Riverside, California 92521, United States

ABSTRACT Ultrasmall gold nanoparticles (*us*-AuNPs, <3 nm) have been recently recognized as surprisingly active and extraordinarily effective green catalysts. Their stability against sintering during reactions, however, remains a serious issue for practical applications. Encapsulating such small nanoparticles in a layer of porous silica can dramatically enhance the stability, but it has been extremely difficult to achieve using conventional sol–gel coating methods due to the weak metal/oxide affinity. In this work, we address this challenge by developing an effective protocol for the synthesis of *us*-AuNP@SiO_2 single-core/shell nanospheres. More specifically, we take an alternative route by starting with ultrasmall gold hydroxide nanoparticles, which have excellent affinity to silica, then carrying out controllable silica coating in reverse micelles, and finally converting gold hydroxide particles into well-protected *us*-AuNPs. With a single-core/shell configuration that prevents sintering of nearby *us*-AuNPs and amino group modification of the Au/SiO_2 interface that provides additional coordinating interactions, the resulting *us*-AuNP@SiO_2 nanospheres are highly stable at high temperatures and show high activity in catalytic CO oxidation reactions. A dramatic and continuous increase in the catalytic activity has been observed when the size of the *us*-AuNPs decreases from 2.3 to 1.5 nm, which reflects the intrinsic size effect of the Au nanoparticles on an inert support. The synthesis scheme described in this work is believed to be extendable to many other ultrasmall metal@oxide nanostructures for much broader catalytic applications.

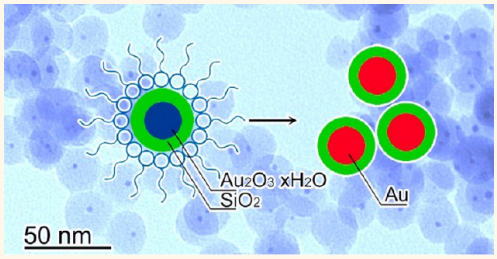

KEYWORDS: gold nanoparticle · silica coating · core/shell nanostructure · reverse micelle · gold hydroxide · CO oxidation

Ultrasmall noble metal nanoparticles, especially Au, have recently garnered a great deal of interest in the field of catalysis due to their size-dependent catalytic activity,[1,2] which makes them particularly useful in CO oxidation[3] and many synthetic reactions.[4] However, these nanoparticles are prone to agglomeration and sintering, leading to drastic loss of catalytic reactivity in a short period of time, especially when an elevated reaction temperature is employed.[5,6] In this regard, it becomes highly desirable to stabilize these ultrasmall catalyst particles on an appropriate support to enhance resistance to sintering and deactivation.

There have been a number of attempts to stabilize noble metal nanoparticles in mesoporous materials.[7−13] As the nanoparticles in these supports are basically in a two-dimensionally confined space, especially when they are positioned in straight columnar mesopores, the nanoparticles can still easily undergo migration or ripening which leads to irreversible sintering when a harsh condition is imposed.[14,15] Alternatively, encapsulation of noble metal nanoparticles in a dielectric material, silica for example, to form a yolk/shell,[16,17] core/shell (with single core or multiple cores),[18−21] or sandwich nanostructure[22−24] has attracted increasing attention, which becomes another remarkable strategy to stabilize these nanoparticles. Among different configurations, the single-core/shell structure is of particular interest, as no neighboring nanoparticles are available for interparticle sintering. In contrast, a core/shell nanosphere containing multiple cores can easily undergo merging of the cores at ambient[21] or elevated

* Address correspondence to gaochuanbo@mail.xjtu.edu.cn, liuhy@imr.ac.cn, yadong.yin@ucr.edu.

Received for review April 30, 2014 and accepted July 1, 2014.

Published online July 01, 2014
10.1021/nn502349k

temperatures (Supporting Information Figure S1) and thus loses the benefit of high active surface area.

Targeting a metal@SiO_2 single-core/shell nanostructure, methods are conventionally adopted such as a modified Stöber process[25−28] and coating within reverse micelles.[29,30] The former only works with metal nanoparticles of a sufficiently large size in a low concentration, making it difficult to achieve large-scale production or be extended to coating nanoparticles with sizes sufficiently small to be of significant interest to the catalysis community. The latter process broadens the size and concentration range of the noble metal nanoparticles to be coated, and therefore, nanoparticles of Au,[31] Pt,[14] Pd,[32−34] and Au/Ni[35] with variable sizes have been successfully encapsulated in silica nanospheres with high yield. However, simple extension of this method for encapsulation of ultrasmall noble metal nanoparticles (<3 nm) to yield a single-core/shell nanostructure has been rarely reported due to a lack of sufficient interaction between the metal nanoparticles and the silicate oligomers.[31]

In this work, we produce silica-encapsulated ultrasmall Au nanoparticles (*us*-AuNPs) by taking an unconventional route. In contrast with earlier reports, our efforts were focused on stabilization of *us*-AuNPs with sizes of less than 3 nm. These nanoparticles are highly active in catalysis, but their stabilization issue has not been well-resolved. In our design, to establish proper nanoparticle/silica interactions, ultrasmall gold hydroxide ($Au_2O_3 \cdot xH_2O$) nanoparticles are synthesized in the first place as precursors to Au nanoparticles, which are expected to have enhanced chemical affinity with silica, analogous to oxide or chalcogenide (Fe_2O_3, CdTe, *etc.*) @SiO_2 cases.[36,37] To reduce the size of the silicate oligomers involved in the silica coating process, a reverse micelle system is employed to confine the hydrolysis and condensation reactions of organosilanes in discrete reverse micelles notwithstanding dynamic intermicelle mass exchange. Small segments of silicate oligomers continuously deposit on the surface of ultrasmall $Au_2O_3 \cdot xH_2O$ nanoparticles to form a single-core/shell configuration. The $Au_2O_3 \cdot xH_2O$ nanoparticles are then conveniently converted into well-protected metallic AuNPs through decomposition in an annealing process. To further enhance the Au/SiO_2 interactions, amino groups are further grafted at their interfaces. Our results show that the resulting *us*-AuNP@SiO_2 nanospheres are highly stable at elevated temperatures, which makes them particularly useful as an efficient catalyst in high-temperature CO oxidation reactions, and the catalytic activity is found to be highly dependent on the size of the encapsulated *us*-AuNPs.

RESULTS AND DISCUSSION

In a typical synthesis, $Au_2O_3 \cdot xH_2O$ nanoparticles were prepared by precipitating $HAuCl_4$ with NH_3 in reverse micelles, which were then coated with silica by introducing organosilanes into the reverse micelle system and allowing their hydrolysis and condensation. The formation of Au(III) hydroxide can be confirmed by X-ray photoelectron spectroscopy (XPS), which will be discussed later. Transmission electron microscopy (TEM) imaging clearly reveals the single-core/shell configuration (Figure 1a). After annealing at 200 °C, which is higher than the decomposition temperature of $Au_2O_3 \cdot xH_2O$ (140 °C to yield Au_2O_3 and 160 °C to yield Au),[38] $Au_2O_3 \cdot xH_2O$ is reduced into metallic Au, giving rise to Au@SiO_2 core/shell nanospheres. This process is accompanied by an obvious color change of the material from yellow to dark brown, indicative of the formation of plasmonic Au nanoparticles. TEM imaging confirms the intact core/shell nanostructure, and that the size of the Au nanoparticles encapsulated in silica nanospheres is close to that before annealing (Figure 1b). It is worth mentioning that an organosilane that contains amino groups (APS) is used to modify the $Au_2O_3 \cdot xH_2O/SiO_2$ interface during the silica coating,[39] which is expected to render the *us*-AuNPs additional coordination interactions with silica and thus improved thermal stability of the *us*-AuNPs in silica nanospheres, as discussed later.

The size of the Au nanoparticle cores, which is critical for their catalytic activities, can be well-tuned by varying the reaction compositions. A typical reaction yields Au@SiO_2 core/shell nanospheres with average core size of 2.3 nm (Figure 1b). By decreasing the concentration of $HAuCl_4$, the precipitation reaction of $HAuCl_4$ with NH_3 produces $Au_2O_3 \cdot xH_2O$ nanoparticles of a smaller size and consequently Au@SiO_2 core/shell nanospheres with a decreased core size (1.8 nm, Figure 1c). By further decreasing the water/oil ratio, the size of the discrete hydrophilic phase becomes even smaller, which eventually affords Au@SiO_2 nanospheres with core size as small as 1.5 nm (Figure 1d). Therefore, this synthesis route is versatile in obtaining Au@SiO_2 core/shell nanospheres with fine-tunable core sizes. The mean silica shell thicknesses of these nanospheres with core sizes of 2.3, 1.8, and 1.5 nm are 11, 10, and 8.6 nm, respectively (Table S1), which are further tunable by simply adjusting the amount of silica source during the synthesis (Figure S2).

The evolution of the Au species in the synthesis of the Au@SiO_2 core/shell nanospheres has been monitored by core-level XPS spectroscopy (Figure 2a,b). The as-prepared sample after precipitation and silica microencapsulation shows clear Au $4f_{7/2}$ and $4f_{5/2}$ photoelectron peaks at binding energies of 86.7 and 90.4 eV, respectively, and these values are typical of a Au(III) species, consistent with the formation of a $Au_2O_3 \cdot xH_2O$ phase.[40] After annealing, the Au $4f_{7/2}$ and $4f_{5/2}$ photoelectron peaks shift to lower values, which are 83.7 and 87.4 eV, respectively, without showing residual signals at their original positions, which confirms that the $Au_2O_3 \cdot xH_2O$ species has been fully

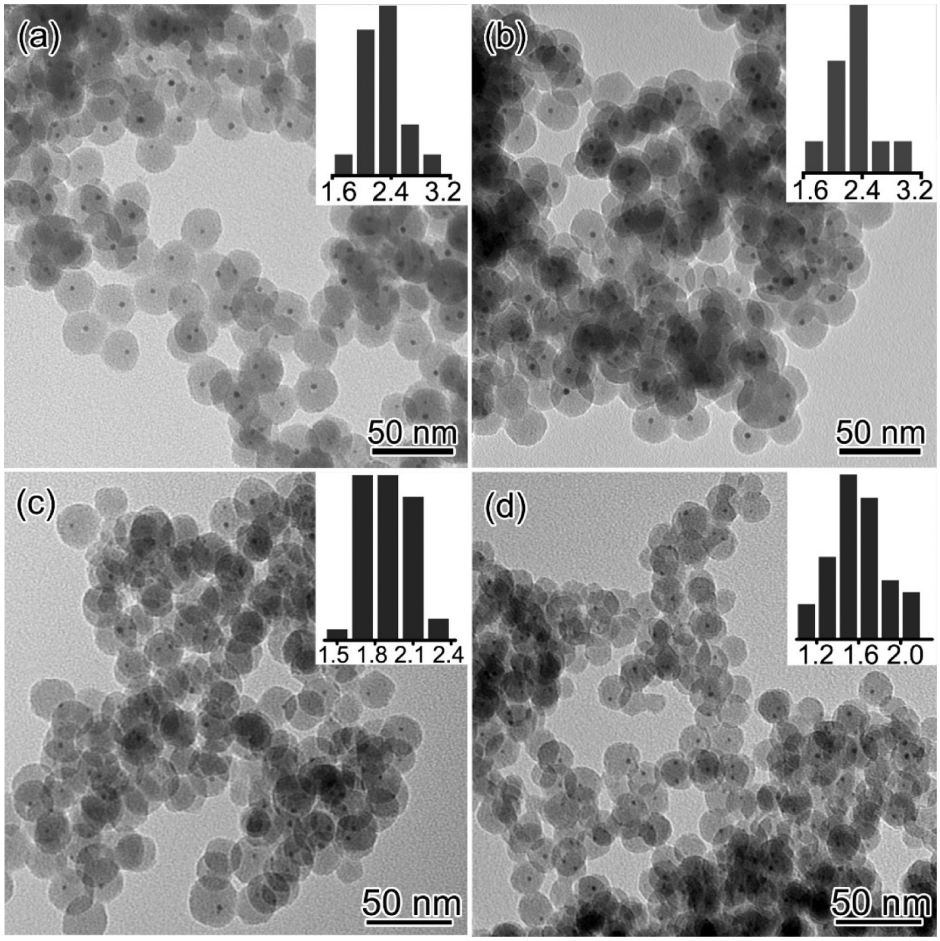

Figure 1. TEM images of the $Au_2O_3 \cdot xH_2O@SiO_2$ and $Au@SiO_2$ core/shell nanospheres. (a) $Au_2O_3 \cdot xH_2O@SiO_2$ nanospheres as prepared with average core size of 2.3 nm. (b–d) $Au@SiO_2$ nanospheres with average core sizes of 2.3, 1.8, and 1.5 nm, respectively, obtained after annealing at 200 °C. Inset: size distributions of the cores in nanometers.

reduced into metallic Au, leading to unambiguous $Au@SiO_2$ core/shell nanospheres.

X-ray diffraction (XRD) patterns of the materials were further investigated to evaluate the crystallinity of the $Au_2O_3 \cdot xH_2O$ and Au nanocrystals in silica nanospheres (Figure 2c). Both spectra show a broad peak at ~23° (2θ) arising from their amorphous silica shells. No extra peaks are observed in the XRD pattern of the $Au_2O_3 \cdot xH_2O@SiO_2$ nanospheres, indicating that it is amorphous. After annealing, peaks emerge with low intensity that can be indexed as {111} and {200} diffractions of Au, which again confirms the formation of metallic Au nanoparticles. The low intensity of the XRD peaks from the $Au@SiO_2$ nanospheres can be ascribed to the small size of the Au nanoparticles such that no long-range periodicity can be detected and to the absence of possible aggregation of Au nanoparticles during the annealing process. The $Au@SiO_2$ core/shell nanospheres thus show pronounced localized surface plasmon resonance at ~523 nm in the UV–vis diffuse reflectance spectrum (Figure 2d), which is broad, as well, due to the strong electron scattering at the Au/dielectric interfaces arising from the ultrasmall sizes.[41]

All of this evidence proves that *us*-AuNPs have been encapsulated in a complete thin layer of silica by the proposed scheme. First, the success relies on the formation of the $Au_2O_3 \cdot xH_2O$ immediate, which possesses much higher chemical affinity with silica compared with bare Au. As a comparison, if the $Au_2O_3 \cdot xH_2O$ nanoparticles in reverse micelles are reduced into Au nanoparticles prior to silica coating, silicate species form free nanospheres instead of growth around Au nanoparticle cores (Figure S3). Second, reverse micelles act as favorable nanoreactors which supply small segments of silicate oligomers for successful coating of silica on the ultrasmall $Au_2O_3 \cdot xH_2O$ nanoparticles. Additionally, reverse micelles also impart high dispersity to these nanoparticles at high concentrations, and thus gram-scale synthesis can be conveniently achieved in the lab (Figure S4). By contrast, a conventional Stöber process conducted in an ethanolic system produces silica nanoparticles decorated with $Au_2O_3 \cdot xH_2O$ nanoparticles instead of $Au_2O_3 \cdot xH_2O@SiO_2$ single-core/shell nanospheres, together with aggregation of the nanoparticles due to the high ionic strength in the coating solution (Figure S3).

In our design, a complete silica shell serves as a physical barrier to effectively prevent the ultrasmall Au nanoparticles from agglomeration. On the other hand,

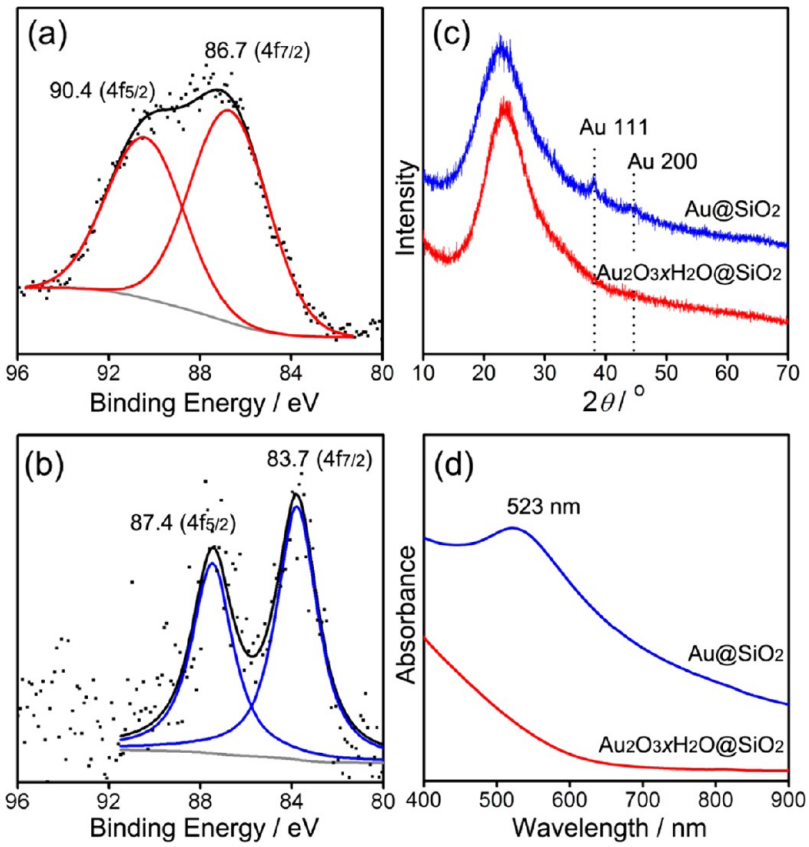

Figure 2. (a,b) XPS spectra of the $Au_2O_3 \cdot xH_2O$@silica and Au@SiO_2 core/shell nanospheres, respectively. Dots and lines represent data as acquired and fitted profiles. (c) XRD patterns. (d) UV−vis diffuse reflectance spectra of the nanospheres. Average core size of the nanospheres is 2.3 nm.

the amorphous silica shell is microporous in nature, showing ~23 m^2/g micropore surface area, which makes the Au nanoparticles accessible in gas-phase catalysis (Figure S5). However, the considerably thin silica shell is not sufficient for limiting migration of the Au atoms at a high temperature, causing growth of some AuNPs at the expense of others (Figure 3 and Figures S6 and S7). To address this issue, an additional mechanism is required to help improve the thermal stability of the ultrasmall Au nanoparticles. We discovered that the stability of the Au nanoparticles in silica nanospheres can be significantly enhanced by introducing amino groups at the core/shell interface. As the coating of silica is accomplished by a layer-by-layer manner, amino group modification can be conveniently achieved by first depositing a layer of APS oligomers before a second layer of silica is deposited. By this means, additional coordination interaction between the *us*-AuNPs (as well as $Au_2O_3 \cdot xH_2O$ nanoparticles before reduction) and the amino groups of the silica shell has been established. As a result, these *us*-AuNPs can survive during the annealing process at 200 °C and remain stable at temperatures up to 500 °C. Figure 4 shows the TEM images and XRD patterns of the Au@SiO_2 core/shell nanospheres with different core sizes which have been annealed at 500 °C for 2 h. It is clear that the core/shell nanostructure is intact, with their core size remaining close to that before annealing. No obvious growth or agglomeration of the Au nanoparticles has been observed. In this sense, these materials are particularly useful in high-temperature catalysis. Besides amino groups, alternative functional groups such as thiols can be grafted at the Au@SiO_2 core/shell interface to provide coordination interaction for sintering resistance, which however appear to be too strong to favor optimal catalytic activities (Figure S8).

The activity of the *us*-Au@SiO_2 single-core/shell nanospheres in CO oxidation is further explored (Figure 5 and Table 1). Figure 5a shows the temperature-dependent catalytic performance of the samples. All the catalysts showed negligible conversion of CO at room temperature. However, as the temperature rose, the conversion of CO rapidly increased and eventually reached ~100%. The smaller the size of the Au nanoparticles, the more rapid increase of the CO conversion was observed. Specifically, samples with core size of 2.3, 1.8, and 1.5 nm reached ~100% conversion at temperatures of ~400, 260, and 180 °C, respectively. It is noteworthy that the same amount of the catalyst (including silica shell) was employed in this experiment, with Au loading determined by inductively coupled plasma mass spectrometry (ICP-MS) to be 2.65, 0.98, and 1.25% for catalysts with core size of 2.3, 1.8, and 1.5 nm, respectively. Although the net amount of Au

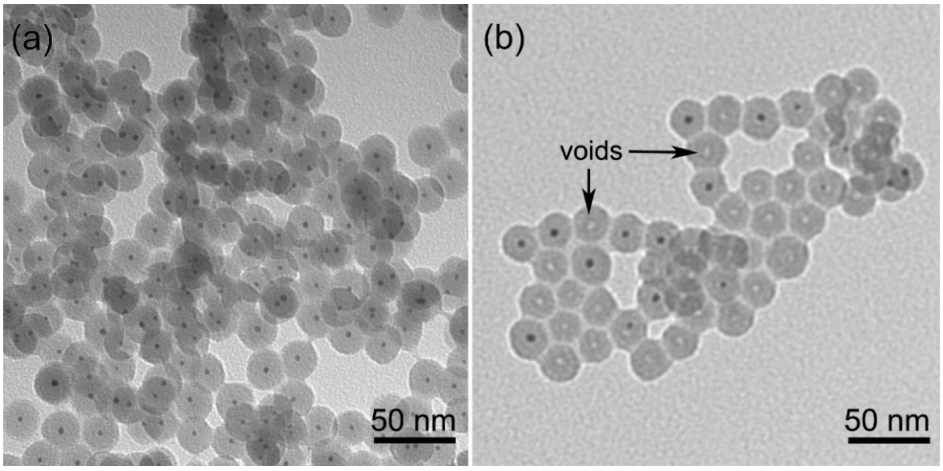

Figure 3. TEM images of the core/shell nanospheres synthesized without addition of APS. (a) $Au_2O_3 \cdot xH_2O@SiO_2$ core/shell nanospheres as synthesized. (b) Sample after reduction by annealing at 200 °C for 2 h.

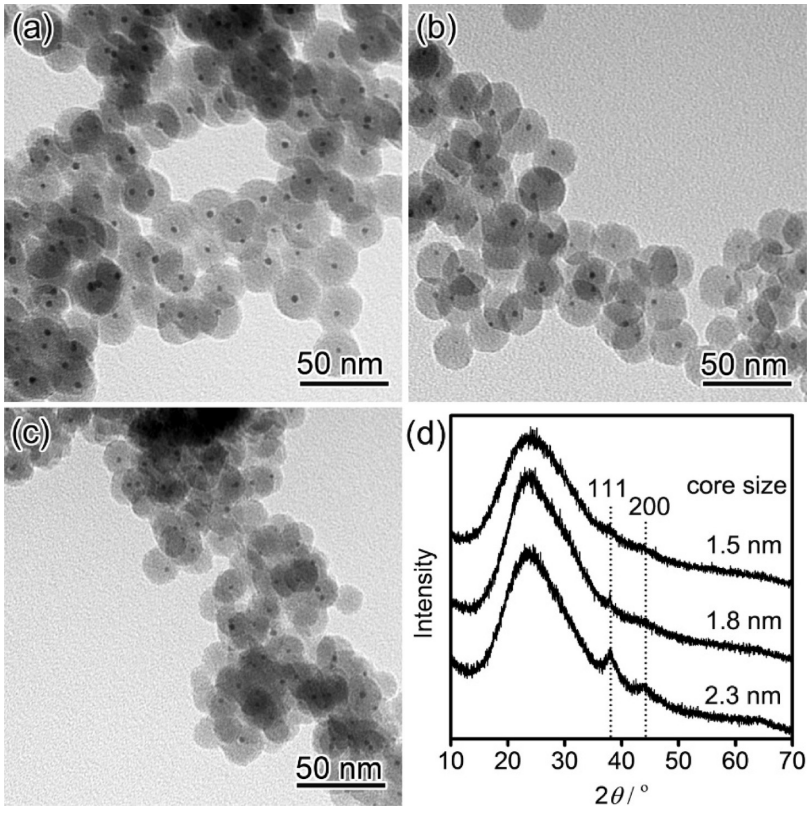

Figure 4. (a–c) TEM images of the $Au@SiO_2$ core/shell nanospheres with average core size of 2.3, 1.8, and 1.5 nm, respectively, after annealing at 500 °C for 2 h. (d) Corresponding XRD patterns of the nanospheres after annealing.

in the catalyst with 1.5 nm cores was only slightly higher than that with 1.8 nm cores, the CO conversion increased several fold compared with that of the latter. At a low temperature of 100 °C, the calculated turnover frequency (TOF) over the $Au@SiO_2$ catalysts with core size of 2.3, 1.8, and 1.5 nm were 6.64, 46.3, and 96.2 h^{-1}, respectively. Therefore, the catalytic activity continuously increases when the size is down to 1.5 nm. This study involves an inert SiO_2 support and confined AuNPs with a narrow size distribution, which suggests that the dramatically enhanced catalytic activity may be attributed to the intrinsic size effect of these novel AuNPs embedded in the SiO_2 support.

Figure 5b–d demonstrates the durability of the $Au@SiO_2$ catalysts in high-temperature catalysis. The catalytic reactions were conducted at their respective threshold temperatures of ~100% conversion. In the 20 h of reaction in our investigation, all the catalysts showed highly stable performance without significant decline, due to the protection of the Au nanoparticles from atomic migration or sintering offered by the robust amino-modified silica shells. For comparison,

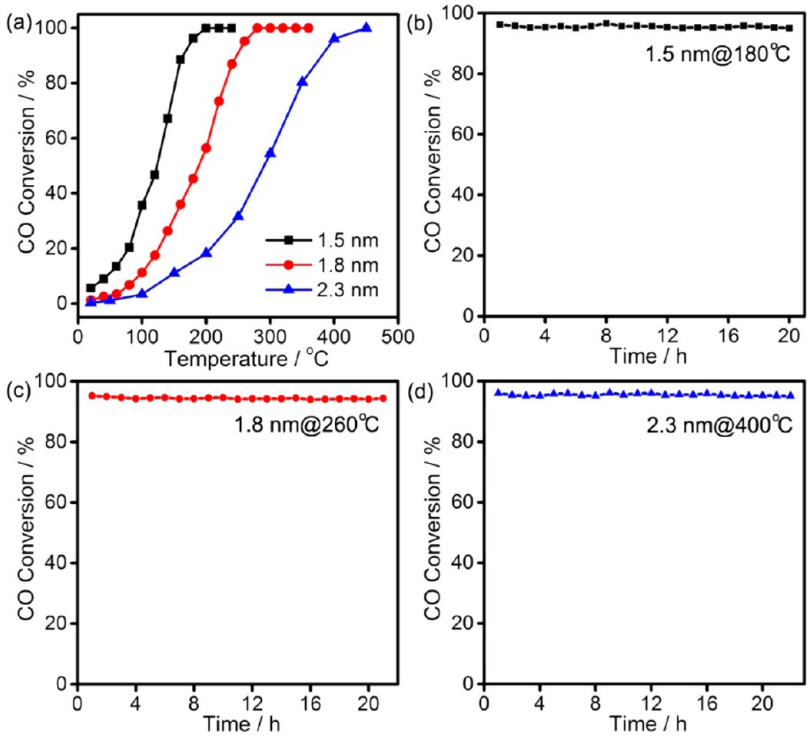

Figure 5. Catalytic CO oxidation of the $Au@SiO_2$ core/shell nanospheres. (a) Plots of CO conversion *versus* reaction temperature when $Au@SiO_2$ of the same amount (in terms of weight) but different core sizes are employed as the catalysts. (b–d) Plots of CO conversion *versus* reaction time. For $Au@SiO_2$ with core sizes of 1.5, 1.8, and 2.3 nm, the catalysis is maintained at 180, 260, and 400 °C, respectively.

TABLE 1. CO Oxidation Activity of the $Au@SiO_2$ Nanospheres with Different Core Sizes

core size	1.5 nm	1.8 nm	2.3 nm
Au content	1.25%	0.98%	2.65%
~100% conversion temperature/°C	≥180	≥260	≥400
TOF (at 100 °C)/h^{-1}	96.2	46.3	6.64

when the *us*-AuNPs were positioned in the columnar pores of SBA-15 mesoporous silica, their activity on CO catalytic oxidation rapidly decreased as a result of particle agglomeration at an elevated working temperature (Figure S9), which is consistent with earlier observations in literature.[15] Therefore, the silica coating method reported in this work represents a more reliable strategy for stabilizing *us*-AuNPs for the purpose of high-temperature catalysis.

In addition, these *us*-AuNP@SiO_2 nanospheres were found to also be active in catalyzing some solution-phase reactions (Figure S10). It is believed that these nanospheres may find much wider use in catalytic applications by creating additional mesopores in the silica shells for better accessibility of the *us*-AuNPs by bulky molecules and extending this synthesis route to many other metal@oxide core/shell nanomaterials (for some examples, see Figure S11).

CONCLUSIONS

In summary, we have developed a synthesis scheme for silica-protected *us*-AuNPs (<3 nm) as efficient catalysts for high-temperature catalysis such as CO oxidation. This process takes advantage of the chemical affinity of $Au_2O_3 \cdot xH_2O$ nanoparticles with silica and a reverse micelle system which is capable of controlling the property of silica oligomers for a successful coating to proceed. The $Au@SiO_2$ single-core/shell nanospheres are highly stable at temperatures up to 500 °C, provided that additional amino group modification of silica is made, which has been demonstrated to show good catalytic performance and durability for high-temperature CO oxidation. Size-dependent catalytic activity of the encapsulated *us*-AuNPs has also been observed. We believe this general synthesis scheme is capable of affording many other ultrasmall metal@oxide nanostructures for a variety of catalytic applications.

METHODS

Synthesis of $Au_2O_3 \cdot xH_2O@SiO_2$ Core/Shell Nanospheres. In a typical synthesis of $Au_2O_3 \cdot xH_2O@SiO_2$ core/shell nanospheres with core size of 2.3 nm, 4.25 g of polyoxyethylene(10) cetyl ether (Brij C10) was dissolved in 7.5 mL of cyclohexane and kept at 50 °C. Then, 0.5 mL of $HAuCl_4$ (0.25 M) was added dropwise under stirring. After a transparent solution was formed, 0.8 mL of $NH_3 \cdot H_2O$ (25%), 150 μL of 3-aminopropyltrimethoxysilane (APS) and 2 mL of tetraethyl orthosilicate (TEOS) were added in order with intervals of 2 min. The reaction was allowed to

proceed for another 2 h, and the product was collected by centrifugation and washed with ethanol.

$Au_2O_3 \cdot xH_2O@SiO_2$ nanospheres with smaller core sizes were synthesized following a similar procedure with modifications. Specifically, nanospheres with core size of 1.8 nm were prepared with 0.2 mL of $HAuCl_4$ (0.25 M), and those with core size of 1.5 nm were prepared with 0.2 mL of $HAuCl_4$ (0.25 M) and 15 mL of cyclohexane, while all the other conditions were kept unchanged.

Synthesis of Au@SiO_2 Core/Shell Nanospheres by Annealing. As a standard procedure, to the $Au_2O_3 \cdot xH_2O@SiO_2$ nanospheres in 20 mL of H_2O was added 1 mL of $NaBH_4$ (0.1 M) for partial reduction of $Au_2O_3 \cdot xH_2O$. The nanospheres were then collected and annealed at 200 °C for 2 h in a muffle furnace for complete conversion of the $Au_2O_3 \cdot xH_2O$ into Au(0). It is noteworthy that the reduction can also be achieved by mere annealing at 200 °C for 2 h in air or H_2 atmosphere (Figure S12).

CO Oxidation. The catalytic activities for CO oxidation were evaluated in a fixed-bed quartz tubular reactor. The reactants were fed with a volume ratio of $He/CO/O_2$ = 79/1/20 (total oxidation). The raw gases were passed over 30 mg of catalyst with a flow rate of 15 mL/min. The gases were determined by Agilent 7890 with a TCD detector.

Characterization. Transmission electron microscopy analysis was performed with a Hitachi HT-7700 microscope equipped with a tungsten filament, operating at 100 kV. X-ray diffraction patterns were recorded on a Rigaku SmartLab Powder X-ray diffractometer equipped with Cu Kα radiation and D/teX Ultra detector, scanning from 10 to 70° (2θ) at the rate of 5°/min. UV–vis diffuse reflectance spectrum was measured with a Shimadzu UV-3600 UV–vis–NIR spectrophotometer. X-ray photoelectron spectroscopy spectra were collected by a Kratos Ultra DLD spectrometer equipped with monochromatic Al Kα radiation. The binding energy scales were calibrated using the C 1s peak at 284.6 eV from carbon contamination. Fitting of the Au 4f core-level spectrum was performed by using two spin–orbit split Au $4f_{7/2}$ and $4f_{5/2}$ components which are separated by 3.7 eV with a fixed area ratio of 4/3. Inductively coupled plasma mass spectrometry was performed with an Agilent 7500CE-ICP-MS for elemental analysis of the materials.

Conflict of Interest: The authors declare no competing financial interest.

Acknowledgment. C.G. gratefully acknowledges support by the National Natural Science Foundation of China (Grant No. 21301138), the Fundamental Research Funds for the Central Universities (xjj2013033), the startup fund, and operational fund for the Center for Materials Chemistry from Xi'an Jiaotong University. H.L. acknowledges support by the National Natural Science Foundation of China (Grant Nos. 21203214 and 21261160487). Y.Y. acknowledges the supports from the U.S. National Science Foundation (CHE-1308587) and U.S. Department of Energy (DE-FG02-09ER16096).

Supporting Information Available: Additional TEM, XRD, XPS, physisorption, and catalysis results. This material is available free of charge *via* the Internet at http://pubs.acs.org.

REFERENCES AND NOTES

1. Roduner, E. Size Matters: Why Nanomaterials Are Different. *Chem. Soc. Rev.* **2006**, *35*, 583–592.
2. Kim, B. H.; Hackett, M. J.; Park, J.; Hyeon, T. Synthesis, Characterization, and Application of Ultrasmall Nanoparticles. *Chem. Mater.* **2014**, *26*, 59–71.
3. Haruta, M.; Kobayashi, T.; Sano, H.; Yamada, N. Novel Gold Catalysts for the Oxidation of Carbon Monoxide at a Temperature Far Below 0 °C. *Chem. Lett.* **1987**, *16*, 405–408.
4. Hashmi, A. S.; Hutchings, G. J. Gold Catalysis. *Angew. Chem., Int. Ed.* **2006**, *45*, 7896–7936.
5. Xin, H. L.; Mundy, J. A.; Liu, Z.; Cabezas, R.; Hovden, R.; Kourkoutis, L. F.; Zhang, J.; Subramanian, N. P.; Makharia, R.; Wagner, F. T.; *et al.* Atomic-Resolution Spectroscopic Imaging of Ensembles of Nanocatalyst Particles across the Life of a Fuel Cell. *Nano Lett.* **2012**, *12*, 490–497.
6. Newton, M. A.; Belver-Coldeira, C.; Martinez-Arias, A.; Fernández-García, M. Dynamic *In Situ* Observation of Rapid Size and Shape Change of Supported Pd Nanoparticles During CO/NO Cycling. *Nat. Mater.* **2007**, *6*, 528–532.
7. Joo, S. H.; Choi, S. J.; Oh, I.; Kwak, J.; Liu, Z.; Terasaki, O.; Ryoo, R. Ordered Nanoporous Arrays of Carbon Supporting High Dispersions of Platinum Nanoparticles. *Nature* **2001**, *412*, 169–172.
8. Sinha, A. K.; Seelan, S.; Tsubota, S.; Haruta, M. A Three-Dimensional Mesoporous Titanosilicate Support for Gold Nanoparticles: Vapor-Phase Epoxidation of Propene with High Conversion. *Angew. Chem., Int. Ed.* **2004**, *43*, 1546–1548.
9. Song, H.; Rioux, R. M.; Hoefelmeyer, J. D.; Komor, R.; Niesz, K.; Grass, M.; Yang, P.; Somorjai, G. A. Hydrothermal Growth of Mesoporous SBA-15 Silica in the Presence of PVP-Stabilized Pt Nanoparticles: Synthesis, Characterization, and Catalytic Properties. *J. Am. Chem. Soc.* **2006**, *128*, 3027–3037.
10. Li, H.; Bian, Z.; Zhu, J.; Huo, Y.; Li, H.; Lu, Y. Mesoporous Au/TiO_2 Nanocomposites with Enhanced Photocatalytic Activity. *J. Am. Chem. Soc.* **2007**, *129*, 4538–4539.
11. Chen, L.; Hu, J.; Richards, R. Intercalation of Aggregation-Free and Well-Dispersed Gold Nanoparticles into the Walls of Mesoporous Silica as a Robust "Green" Catalyst for *N*-Alkane Oxidation. *J. Am. Chem. Soc.* **2009**, *131*, 914–915.
12. Wu, P.; Bai, P.; Lei, Z.; Loh, K. P.; Zhao, X. S. Gold Nanoparticles Supported on Functionalized Mesoporous Silica for Selective Oxidation of Cyclohexane. *Microporous Mesoporous Mater.* **2011**, *141*, 222–230.
13. Jin, Z.; Xiao, M.; Bao, Z.; Wang, P.; Wang, J. A General Approach to Mesoporous Metal Oxide Microspheres Loaded with Noble Metal Nanoparticles. *Angew. Chem., Int. Ed.* **2012**, *51*, 6406–6410.
14. Joo, S. H.; Park, J. Y.; Tsung, C. K.; Yamada, Y.; Yang, P.; Somorjai, G. A. Thermally Stable Pt/Mesoporous Silica Core–Shell Nanocatalysts for High-Temperature Reactions. *Nat. Mater.* **2009**, *8*, 126–131.
15. Yang, C.-M.; Kalwei, M.; Schüth, F.; Chao, K.-J. Gold Nanoparticles in SBA-15 Showing Catalytic Activity in CO Oxidation. *Appl. Catal. A* **2003**, *254*, 289–296.
16. Lee, I.; Joo, J. B.; Yin, Y.; Zaera, F. A Yolk@Shell Nanoarchitecture for Au/TiO_2 Catalysts. *Angew. Chem., Int. Ed.* **2011**, *50*, 10208–10211.
17. Wu, S.-H.; Tseng, C.-T.; Lin, Y.-S.; Lin, C.-H.; Hung, Y.; Mou, C.-Y. Catalytic Nano-Rattle of Au@Hollow Silica: Towards a Poison-Resistant Nanocatalyst. *J. Mater. Chem.* **2011**, *21*, 789–794.
18. Ghosh Chaudhuri, R.; Paria, S. Core/Shell Nanoparticles: Classes, Properties, Synthesis Mechanisms, Characterization, and Applications. *Chem. Rev.* **2012**, *112*, 2373–2433.
19. Yadav, M.; Akita, T.; Tsumori, N.; Xu, Q. Strong Metal–Molecular Support Interaction (SMMSI): Amine-Functionalized Gold Nanoparticles Encapsulated in Silica Nanospheres Highly Active for Catalytic Decomposition of Formic Acid. *J. Mater. Chem.* **2012**, *22*, 12582–12586.
20. Pak, J.; Yoo, H. Facile Synthesis of Spherical Nanoparticles with a Silica Shell and Multiple Au Nanodots as the Core. *J. Mater. Chem. A* **2013**, *1*, 5408–5413.
21. Pak, J.; Yoo, H. Synthesis and Catalytic Performance of Multiple Gold Nanodots Core–Mesoporous Silica Shell Nanoparticles. *Microporous Mesoporous Mater.* **2014**, *185*, 107–112.
22. Ge, J.; Zhang, Q.; Zhang, T.; Yin, Y. Core-Satellite Nanocomposite Catalysts Protected by a Porous Silica Shell: Controllable Reactivity, High Stability, and Magnetic Recyclability. *Angew. Chem., Int. Ed.* **2008**, *47*, 8924–8928.
23. Zhang, Q.; Lee, I.; Ge, J.; Zaera, F.; Yin, Y. Surface-Protected Etching of Mesoporous Oxide Shells for the Stabilization of Metal Nanocatalysts. *Adv. Funct. Mater.* **2010**, *20*, 2201–2214.
24. Zhang, Q.; Lima, D. Q.; Lee, I.; Zaera, F.; Chi, M.; Yin, Y. A Highly Active Titanium Dioxide Based Visible-Light Photocatalyst with Nonmetal Doping and Plasmonic Metal Decoration. *Angew. Chem., Int. Ed.* **2011**, *50*, 7088–7092.

25. Zhu, X.; Wu, L.; Mungra, D. C.; Xia, S.; Zhu, J. Au@SiO_2 Core−Shell Nanoparticles for Laser Desorption/Ionization Time of Flight Mass Spectrometry. *Analyst* **2012**, *137*, 2454–2458.
26. Graf, C.; Vossen, D. L. J.; Imhof, A.; van Blaaderen, A. A General Method To Coat Colloidal Particles with Silica. *Langmuir* **2003**, *19*, 6693–6700.
27. Ung, T.; Liz-Marzán, L. M.; Mulvaney, P. Controlled Method for Silica Coating of Silver Colloids. Influence of Coating on the Rate of Chemical Reactions. *Langmuir* **1998**, *14*, 3740–3748.
28. Liz-Marzán, L. M.; Giersig, M.; Mulvaney, P. Synthesis of Nanosized Gold−Silica Core−Shell Particles. *Langmuir* **1996**, *12*, 4329–4335.
29. Wang, J.; Shah, Z. H.; Zhang, S.; Lu, R. Silica-Based Nanocomposites *via* Reverse Microemulsions: Classifications, Preparations, and Applications. *Nanoscale* **2014**, *6*, 4418–4437.
30. Gao, C.; Lu, Z.; Yin, Y. Gram-Scale Synthesis of Silica Nanotubes with Controlled Aspect Ratios by Templating of Nickel-Hydrazine Complex Nanorods. *Langmuir* **2011**, *27*, 12201–12208.
31. Han, Y.; Jiang, J.; Lee, S. S.; Ying, J. Y. Reverse Microemulsion-Mediated Synthesis of Silica-Coated Gold and Silver Nanoparticles. *Langmuir* **2008**, *24*, 5842–5848.
32. Bae, D.-S.; Han, K.-S.; Adair, J. H. Synthesis and Microstructure of Pd/SiO_2 Nanosized Particles by Reverse Micelle and Sol−Gel Processing. *J. Mater. Chem.* **2002**, *12*, 3117–3120.
33. Park, J. C.; Heo, E.; Kim, A.; Kim, M.; Park, K. H.; Song, H. Extremely Active Pd@pSiO_2 Yolk−Shell Nanocatalysts for Suzuki Coupling Reactions of Aryl Halides. *J. Phys. Chem. C* **2011**, *115*, 15772–15777.
34. Hu, Y.; Tao, K.; Wu, C.; Zhou, C.; Yin, H.; Zhou, S. Size-Controlled Synthesis of Highly Stable and Active Pd@SiO_2 Core−Shell Nanocatalysts for Hydrogenation of Nitrobenzene. *J. Phys. Chem. C* **2013**, *117*, 8974–8982.
35. Jiang, H. L.; Umegaki, T.; Akita, T.; Zhang, X. B.; Haruta, M.; Xu, Q. Bimetallic Au−Ni Nanoparticles Embedded in SiO_2 Nanospheres: Synergetic Catalysis in Hydrolytic Dehydrogenation of Ammonia Borane. *Chem.—Eur. J.* **2010**, *16*, 3132–3137.
36. Yang, Y.; Gao, M. Y. Preparation of Fluorescent SiO_2 Particles with Single CdTe Nanocrystal Cores by the Reverse Microemulsion Method. *Adv. Mater.* **2005**, *17*, 2354–2357.
37. Selvan, S. T.; Patra, P. K.; Ang, C. Y.; Ying, J. Y. Synthesis of Silica-Coated Semiconductor and Magnetic Quantum Dots and Their Use in the Imaging of Live Cells. *Angew. Chem., Int. Ed.* **2007**, *46*, 2448–2452.
38. Nekrasov, I. Y. *Geochemistry, Mineralogy and Genesis of Gold Deposits*; CRC Press: Boca Raton, FL, 1996; p 118.
39. Gao, C.; Zhang, Q.; Lu, Z.; Yin, Y. Templated Synthesis of Metal Nanorods in Silica Nanotubes. *J. Am. Chem. Soc.* **2011**, *133*, 19706–19709.
40. Casaletto, M. P.; Longo, A.; Martorana, A.; Prestianni, A.; Venezia, A. M. XPS Study of Supported Gold Catalysts: The Role of Au^0 and $Au^{+\delta}$ Species as Active Sites. *Surf. Interface Anal.* **2006**, *38*, 215–218.
41. Link, S.; El-Sayed, M. A. Spectral Properties and Relaxation Dynamics of Surface Plasmon Electronic Oscillations in Gold and Silver Nanodots and Nanorods. *J. Phys. Chem. B* **1999**, *103*, 8410–8426.